

# Lithium Hydrazinidoborane: A Polymorphic Material with Potential for Chemical Hydrogen Storage

Romain Moury,<sup>†</sup> Umit B. Demirci,<sup>\*,†</sup> Voraksmy Ban,<sup>‡</sup> Yaroslav Filinchuk,<sup>‡</sup> Takayuki Ichikawa,<sup>§</sup> Liang Zeng,<sup>||</sup> Kiyotaka Goshome,<sup>||</sup> and Philippe Miele<sup>†</sup>

<sup>†</sup>IEM (Institut Européen des Membranes), UMR5635 (CNRS, ENSCM, UM2), Université Montpellier 2, Place Eugene Bataillon, CC047, F-34095, Montpellier, France

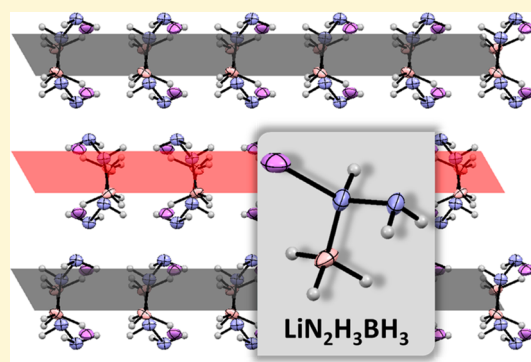
<sup>‡</sup>Institute of Condensed Matter and Nanosciences, Université Catholique de Louvain, Place L. Pasteur 1, 1348 Louvain-la-Neuve, Belgium

<sup>§</sup>Institute for Advanced Materials Research, Hiroshima University, 1-3-1 Kagamiyama, Higashi-Hiroshima, 739-8530, Japan

<sup>||</sup>Graduate School of Advanced Sciences of Matter, Hiroshima University, 1-3-1 Kagamiyama, Higashi-Hiroshima, 739-8530, Japan

## Supporting Information

**ABSTRACT:** Herein, we describe the synthesis and characterization (chemical, structural, and thermal) of a new crystal phase of lithium hydrazinidoborane ( $\text{LiN}_2\text{H}_4\text{BH}_3$ , LiHB), which is a new material for solid-state chemical hydrogen storage. We put in evidence that lithium hydrazinidoborane is a polymorphic material, with a stable low-temperature phase and a metastable high-temperature phase. The former is called  $\beta$ -LiHB and the latter  $\alpha$ -LiHB. Results from DSC and XRD showed that the transition phase occurs at around 90 °C. On this basis, the crystal structure of the novel  $\beta$ -LiHB phase was solved. The potential of this material for solid-state chemical hydrogen storage was verified by TGA, DSC, and isothermal dehydrogenations. Upon the formation of the  $\alpha$ -LiHB phase, the borane dehydrogenates. At 150 °C, it is able to generate 10 wt % of pure  $\text{H}_2$  while a solid residue consisting of polymers with linear and cyclic units forms. Reaction mechanisms and formation of bis(lithium hydrazide) of diborane  $[(\text{LiN}_2\text{H}_3)_2\text{BH}_2]^+[\text{BH}_4]^-$  as a reaction intermediate are tentatively proposed to highlight the decomposition of  $\beta$ -LiHB in our conditions.



## INTRODUCTION

Solid-state chemical hydrogen storage is a recent field in material science and has shown to have high potential to address the storage issue of the near-future hydrogen economy.<sup>1</sup> Technically, the ultimate objective is to find a way to store hydrogen safely and in high amounts.<sup>2</sup>

In this context, boron- and/or nitrogen-based materials, though not storing hydrogen reversibly, have shown to be very attractive candidates for carrying high amounts of hydrogen, which is of high interest for some (military and niche) applications. Ammonia borane  $\text{NH}_3\text{BH}_3$  (AB) is a typical example: (i) it is stable in ambient conditions if kept under an argon atmosphere,<sup>3</sup> and (ii) it is composed of 3  $\text{H}^{\delta+}$  and 3  $\text{H}^{\delta-}$  per 1 B and 1 N, and theoretically stores 19.6 wt % H. Accordingly, AB meets the aforementioned criteria for suitability in solid-state chemical hydrogen storage.<sup>4</sup>

Ammonia borane is stable upon heating at a constant rate up to ca. 100 °C, the temperature at which it starts to decompose.<sup>5</sup> However, over the temperature range of 100–200 °C, AB loses 40–60 wt % because of the release of  $\text{H}_2$ , but also of unwanted gaseous byproducts, such as borazine  $\text{B}_3\text{N}_3\text{H}_6$ , diborane  $\text{B}_2\text{H}_6$ , and aminoborane  $\text{NH}_2\text{BH}_2$ .<sup>5,6</sup> The thermolytic decomposition

suffers thus from two main drawbacks: a high onset temperature of dehydrogenation and the impurity of the released  $\text{H}_2$ . To solve these issues, various strategies of AB destabilization have been considered so far.<sup>7</sup> One of them focuses on chemical modification of AB to get derivatives that are less stable than the parent material. For example, Xiong et al. synthesized metal amidoboranes  $\text{MNH}_2\text{BH}_3$  (MAB) by ball-milling AB and an alkaline hydride MH (with  $\text{M} = \text{Li}$  and  $\text{Na}$ ), and demonstrated the positive effect of such a destabilization with an onset temperature of dehydrogenation decreased to ca. 60 °C and liberation of  $\text{H}_2$  without borazine.<sup>8</sup> However, for sodium amidoborane  $\text{NaNH}_2\text{BH}_3$ , Fijalkowski et al. reported emission of ammonia.<sup>9</sup>

Recently, hydrazine borane  $\text{N}_2\text{H}_4\text{BH}_3$  (HB), another boron- and nitrogen-based material, emerged. It has been presented as an alternative to AB.<sup>10</sup> HB has a gravimetric capacity of 15.3 wt % H. Upon heating at 5 °C  $\text{min}^{-1}$ , it decomposes from ca. 60 °C.<sup>10,11</sup> In a previous work,<sup>11</sup> we showed that, over the range of

Received: March 20, 2014

Revised: May 5, 2014

Published: May 6, 2014

60–95 °C, HB loses 1.2 wt % of pure H<sub>2</sub>, but from 95 °C, the mass loss is significant, due to emission of hydrazine and/or ammonia. Unlike AB, no trace of borazine is detected. Actually, the situation is similar to that faced with AB: the challenges with HB are to decrease the onset temperature of dehydrogenation while avoiding the release of unwanted byproducts.

Wu et al. and then our group proposed to destabilize HB by ball-milling the borane in the presence of an equimolar amount of LiH and NaH, respectively.<sup>12,13</sup> Therefore, Wu et al. synthesized lithium hydrazinidoborane LiN<sub>2</sub>H<sub>3</sub>BH<sub>3</sub> (LiHB; 11.6 wt % H).<sup>12</sup> We successfully prepared sodium hydrazinidoborane NaN<sub>2</sub>H<sub>3</sub>BH<sub>3</sub> (NaHB; 8.8 wt % H).<sup>13</sup> Both materials possess 3 H<sup>δ-</sup> in tandem with 3 H<sup>δ+</sup>, and they could theoretically release up to 3 mol of H<sub>2</sub> per mole of metal hydrazinidoborane. In practical terms, LiN<sub>2</sub>H<sub>3</sub>BH<sub>3</sub> is able to liberate 9.3 wt % of H<sub>2</sub> under heating at 130 °C for 1 h,<sup>12</sup> and NaN<sub>2</sub>H<sub>3</sub>BH<sub>3</sub> releases 8.1 wt % of H<sub>2</sub> with very fast desorption kinetics when heated at 100 °C for 1 h.<sup>13</sup> Accordingly, both boranes have attractive features for solid-state chemical hydrogen storage.

In 2012, when Wu et al. published their work on LiHB,<sup>12</sup> we were also working on the mechanosynthesis of this material from lab-made HB and commercial LiH. However, we were triggering repeatability problems with our successive syntheses. Finally, we evidenced the formation of two polymorphs of LiHB in this system. Hence, we report herein the mechanochemical synthesis procedure, characterization results, and thermal and dehydrogenation properties of a new crystal phase of LiHB. We have called the Wu et al.'s phase  $\alpha$ -LiHB and our new phase  $\beta$ -LiHB.

## EXPERIMENTAL DETAILS

**Materials and Synthesis.** Commercial sodium borohydride NaBH<sub>4</sub> (Acros, 99%), hydrazine hemisulfate N<sub>2</sub>H<sub>4</sub>·1/2(SO<sub>4</sub>) (Aldrich, >99%), anhydrous 1,4-dioxane (Sigma-Aldrich, >99%), and lithium hydride LiH (Sigma-Aldrich, 95%) were used as-received. They were stored and handled in an argon-filled glovebox (MBraun M200B, H<sub>2</sub>O ≤ 0.1 ppm, O<sub>2</sub> ≤ 0.1 ppm). The solvent was used under an argon flow. HB was synthesized following a procedure we had optimized.<sup>11</sup> Typically, sodium borohydride and hydrazine hemisulfate were introduced in a round-bottom Schlenk glassware, followed by 1,4-dioxane. The slurry was kept under stirring during 48 h in ambient conditions. Then, the reaction mixture was filtered off and the filtrate was dried under vacuum. HB with a purity of ≥99% was obtained and stored in the glovebox. The synthesis of  $\beta$ -LiHB was performed by mechanochemical synthesis. In the argon-filled glovebox, equimolar amounts of HB and LiH were transferred in a stainless steel grinding jar. The weight ratio of balls over reactants (denoted R) was set at 200:1. After sealing, the jar was removed outside the glovebox, and the mixture was ball-milled by using a RETSCH PM 100 planetary ball mill. The milling conditions were optimized to the following parameters: 10 min of milling, followed by a 20 min break, 18 times, 200 rpm, and at ambient conditions. Finally, the jar was transferred into the glovebox and the sample recovered by sieving. The as-synthesized  $\beta$ -LiHB was stored and handled in the glovebox. For comparison with  $\beta$ -LiHB,  $\alpha$ -LiHB was prepared. Equimolar amounts of LiH and HB were put in a stainless steel grinding jar in the glovebox such as R = 200:1. Two milling cycles were necessary. During the first one, the mixture was ball-milled for 10 min, followed by a break of 10 min; this was done 10 times at 200 rpm at ambient conditions. The solid was recovered by sieving in the glovebox. The second cycle was performed as follows: 10 min of milling, 50 min of break, 18 times, 300 rpm, at ambient conditions. The as-obtained  $\alpha$ -LiHB was recovered by sieving in the glovebox. The XRD pattern is shown in Figure 2a and is compared to that of  $\beta$ -LiHB.

**Characterizations.** The crystal structure of  $\beta$ -LiHB (loaded in a 0.5 mm diameter glass capillary under an inert atmosphere) was analyzed by powder X-ray diffraction (XRD) with synchrotron radiation at the ESRF at the BM01 beamline (SNBL). The wavelength was  $\lambda = 0.69405$  Å. A 2D detector Pilatus 2 M positioned at 411 mm from the sample was used, and the detector geometry was calibrated with a LaB<sub>6</sub> standard. The molecular structure of  $\beta$ -LiHB was analyzed by Fourier transform infrared (FTIR) spectroscopy (Nicolet 710, 32 scans) and by <sup>11</sup>B MAS NMR (Varian VNMR400, 128.37 MHz). Thermogravimetric analyses (TGA) were performed using Rigaku TG8120 coupled with an M-QA200TS mass spectrometer under helium flux. The measurement was directly recorded inside an argon-filled glovebox. About 3 mg of product was loaded in a platinum crucible and then analyzed with a heating rate of 2 °C min<sup>-1</sup>. The same experimental conditions were used for differential scanning calorimetry (DSC, TA Instruments, Q10PDS). Thermal behavior under prolonged heating at constant temperature (90, 110, 140, and 150 °C) was investigated with our lab-made bench. The sample in a round-bottom Schlenk flask was heated by immersing the glassware in a thermostated oil bath. The volume of H<sub>2</sub> was followed with an inverted buret filled with colored water, the volume variation being video-recorded and afterward plotted using the Matlab software. Between the Schlenk flask and the inverted buret, a cold trap (kept at 0 °C) and a Dräger tube were placed in order to condensate any evolving hydrazine and to trap ammonia, respectively. The purity of H<sub>2</sub> after isothermal treatment was investigated by gas chromatography (Shimadzu, GC-14B; Column Chromosorb 103 (porous polymer adsorbent); 40 °C; Detector TCD). For both H<sub>2</sub> and NH<sub>3</sub>, 2250 points were recorded every 0.4 s for 15 min; the retention times were 1.57 and 5.57 min, respectively.

## RESULTS AND DISCUSSION

**Molecular Structure of  $\beta$ -LiHB.** The FTIR spectrum of  $\beta$ -LiHB is displayed in Figure 1a. The fingerprint of the N–H stretching bands (3390–3070 cm<sup>-1</sup>) of  $\beta$ -LiHB is less complex than that observed for HB (3500–2600 cm<sup>-1</sup>). This suggests that the N–H bonds of the hydrazinidoborane are involved in a smaller number of N–H···H–B interactions. The H<sup>δ+</sup>···H<sup>δ-</sup> network within  $\beta$ -LiHB should be weaker, which is a sign of decreased stability in comparison to HB. This effect is confirmed by the broadened N–H bending and rocking bands (1300–1800 cm<sup>-1</sup>). With respect to the B–H stretching region (2480–1900 cm<sup>-1</sup>), there are more bands, especially at lower wavenumbers than for HB (2500–2100 cm<sup>-1</sup>).

The Li<sup>+</sup> cation would interact with the H<sup>δ-</sup> of the BH<sub>3</sub> group, leading to different environments for the B–H bonds. The polarization of these bonds, and thus their reactivity, should have changed in comparison to HB. Concerning the N–N and B–N stretching regions for  $\beta$ -LiHB, the bands have red- and blue-shifted, respectively:  $\nu(\text{N–N}) = 1050$  cm<sup>-1</sup> and  $\nu(\text{B–N}) = 748$  cm<sup>-1</sup> for  $\beta$ -LiHB vs  $\nu(\text{N–N}) = 1022$  cm<sup>-1</sup> and  $\nu(\text{B–N}) = 781$  cm<sup>-1</sup> for HB. This is indicative of weaker N–N and stronger B–N bonds for  $\beta$ -LiHB. This reveals a strong electronic modification induced by the alkaline cation, as reported elsewhere.<sup>8,9,12,13</sup> Armstrong et al. reported that the formation of Li<sup>+</sup>···H<sup>δ-</sup> long-range interactions results in the increase of the Lewis basicity of the NH<sub>3</sub> moiety in AB derivatives,<sup>14</sup> which supports the strengthening we have predicted from the FTIR results.

Figure 1b shows the <sup>11</sup>B MAS NMR spectrum of  $\beta$ -LiHB. The signal of boron of  $\beta$ -LiHB is centered at –19.1 ppm and shows a single environment. Unlike in pristine HB, there is no quadrupolar effect, which could potentially be due to an interaction among the two quadrupolar elements: <sup>11</sup>B with  $s = 3/2$  and <sup>7</sup>Li with  $s = 3/2$ . No quadrupolar interaction was observed in NaHB.<sup>13</sup> These observations demonstrate that the

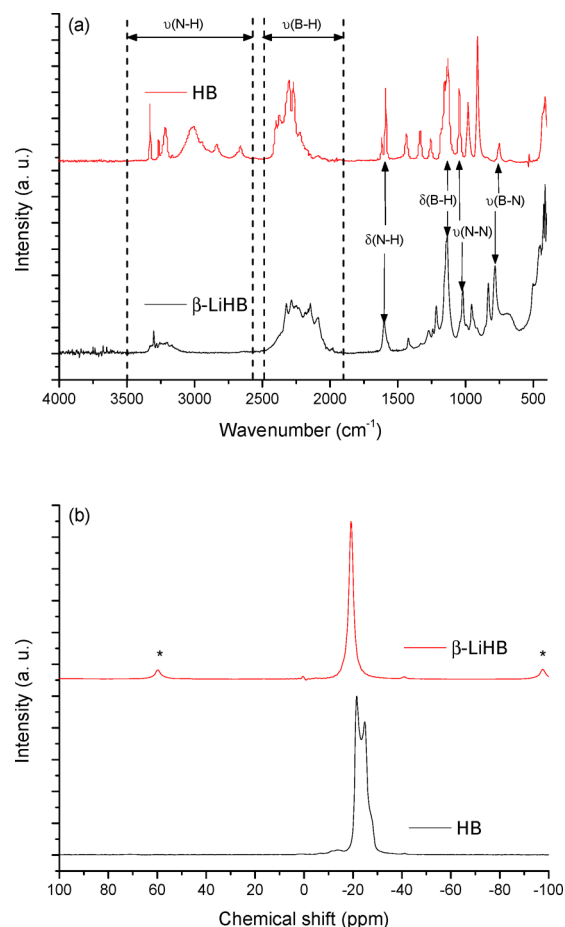


**Figure 1.** (a) FTIR and (b)  $^{11}\text{B}$  MAS NMR (the spinning sidebands are indicated by \*) spectra for  $\beta$ -LiHB and HB.

units in the crystal of  $\beta$ -LiHB are all equivalent and the insertion of the lithium modifies notably the electron repartition around the boron, which has become isotropic.

**Crystal Structure of  $\beta$ -LiHB.** The XRD pattern of  $\beta$ -LiHB was indexed as a single phase using an orthorhombic  $Pbca$  (No. 61) space group with  $a = 10.25182(11)$  Å,  $b = 8.47851(10)$  Å, and  $c = 7.46891(8)$  Å. The crystal structure was solved by global optimization with a parallel tempering algorithm using FOX software,<sup>15</sup> and then refined with the Rietveld method, anisotropically for non-H atoms, in the JANA2006 software.<sup>16</sup> After refinement, the following agreement factors were obtained:  $R_p = 2.3\%$ ;  $R_{wp} = 5.9\%$  (conventional);  $GOF = 9.02$ . The calculated pattern was then compared to the experimental one and both matched (Figure 2b).

Furthermore, removal of only one H atom in this light-Z system results in an increase of GOF up to 13. This assumption was confirmed by the refinement of the H positions, which lead to the expected staggered configuration on the  $sp^3$ -hybridized pivot (Figure 3). Despite the high sensitivity of synchrotron X-rays to H atoms in light hydrides,<sup>17</sup> only the average position of the electron cloud can be determined.

Accordingly, a systematic correction for the position of the H elements was introduced by extending the lengths of the B–H and N–H bonds to the ideal values of 1.22 and 1.03 Å, respectively.<sup>18</sup> The resulting coordinates are listed in Table S1 (Supporting Information). The crystal structure illustrated in Figure 4 shows that  $\text{H}^{\delta-}$  of LiH reacted with  $\text{H}^{\delta+}$  of the central nitrogen of HB (Figure 4a), leading to the formation of the new

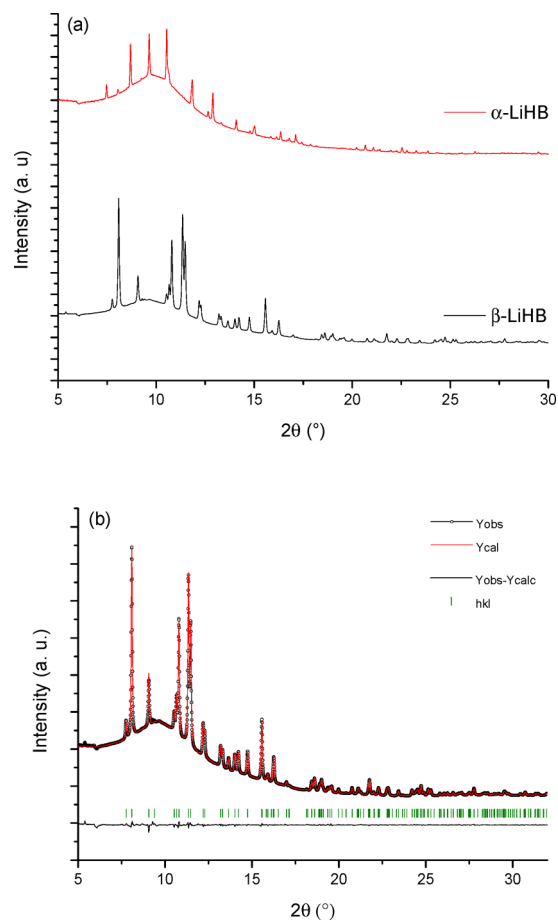


**Figure 2.** (a) High-resolution XRD patterns ( $\lambda = 0.693203$  Å) of the two phases of LiHB, i.e.,  $\alpha$ -LiHB and  $\beta$ -LiHB. (b) Comparison of the calculated (red line) and experimental (black circles) patterns. The difference is shown by the black line. The green vertical bars represent the calculated position of Bragg peaks for the  $\beta$ -LiHB phase.

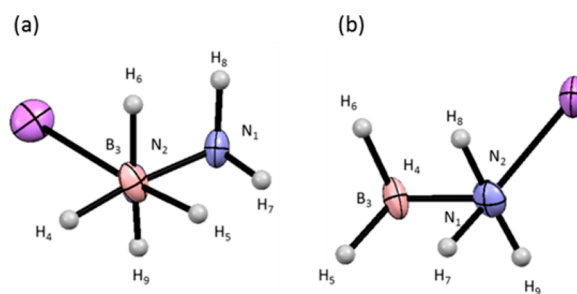


**Figure 3.** Representation of the staggered conformation for H on the  $sp^3$  pivot: (a) along the  $\text{N}_2$ – $\text{B}_3$  bond and (b) along the  $\text{N}_2$ – $\text{N}_1$  bond.

crystal phase of LiHB and  $\text{H}_2$ . This mode of deprotonation is consistent with those observed in the compounds NaHB and  $\alpha$ -LiHB and the complex LiHB·2HB.<sup>12,13</sup>

Figure 4b shows that  $\text{Li}^+$  has a tetrahedral environment: it interacts with four  $\text{N}_2\text{H}_3\text{BH}_3^-$  entities. A tetrahedral coordination polyhedron is typical for the metal atom in ambient pressure phases of lithium borohydride  $\text{LiBH}_4$ .<sup>18</sup> Two corners of the tetrahedron are occupied by  $\text{BH}_3$  groups ( $\text{B}_3 \cdots \text{Li}^+$ : 2.624(5) and 2.622(6) Å), and the interaction occurs through the  $\text{BH}_2$  edge. Consequently,  $\text{Li}^+$  modifies the B–H bond polarization and decreases the electronic density around the B atoms, which explains the observations made by FTIR (Figure

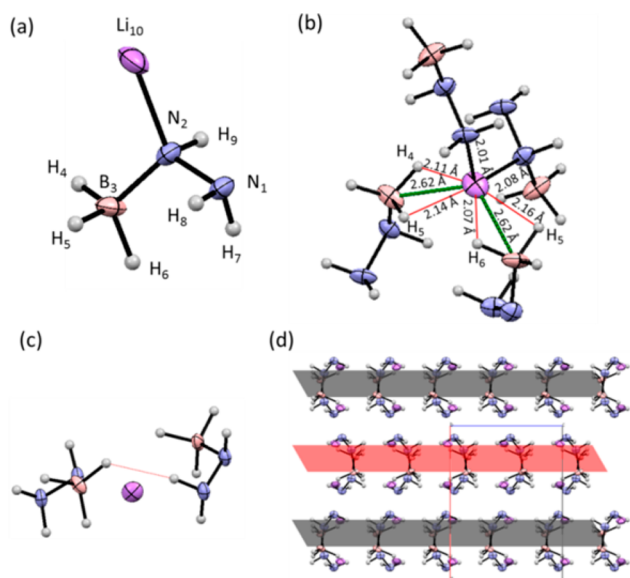


**Figure 4.** Crystal structure of  $\beta$ -LiHB with a detailed view of: (a) the asymmetric unit with labels; (b) the coordination of  $\text{Li}^+$ ; (c) the intermolecular  $\text{H}^{\delta+}\cdots\text{H}^{\delta-}$  dihydrogen bond according to Klooster et al.'s definition<sup>20</sup> ( $\text{H}_4\cdots\text{H}_7 = 2.25$  Å,  $\text{B}_3\text{-H}_4\cdots\text{H}_7 = 106.8^\circ$ , and  $\text{N}_1\text{-H}_7\cdots\text{H}_4 = 171.2^\circ$ ); and (d) the representation of the parallel planes on which the  $\text{H}^{\delta+}\cdots\text{H}^{\delta-}$  network extends.

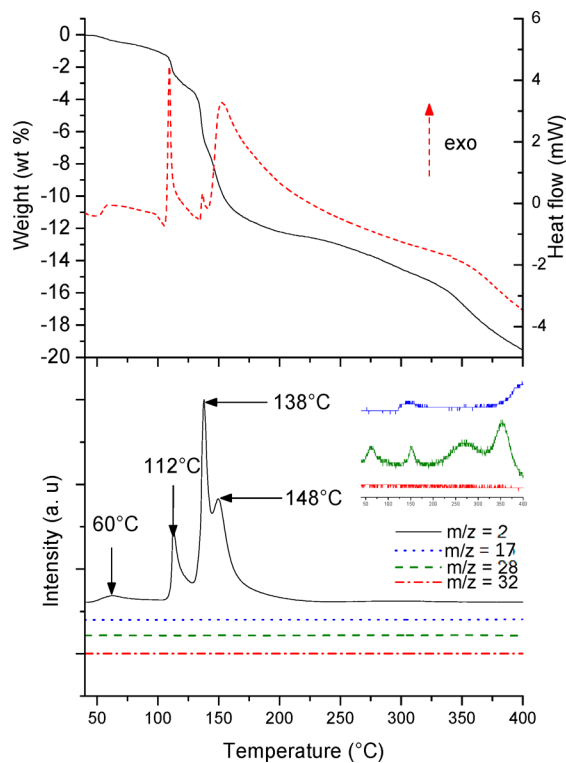


**Figure 5.** TGA/DSC ( $2^\circ\text{C min}^{-1}$ ) and MS results of  $\beta$ -LiHB: with  $m/z = 2$  for  $\text{H}_2$ ,  $m/z = 17$  for  $\text{NH}_3$ ,  $m/z = 28$  for  $\text{N}_2$ , and  $m/z = 32$  for  $\text{N}_2\text{H}_4$ . For the MS results, the inset is a zoom ( $\times 1000$ ) for the gases  $\text{NH}_3$ ,  $\text{N}_2$ , and  $\text{N}_2\text{H}_4$ .

1a) and confirms the  $\text{Li}^+\cdots\text{H}^{\delta-}$  interactions. This effect should lead to an activation of  $\text{H}^{\delta-}$  and, therefore, to an increase of its reactivity.<sup>19</sup> On the other hand,  $\text{Li}^+$  is coordinated with two N atoms from two different anions. The first coordination is done

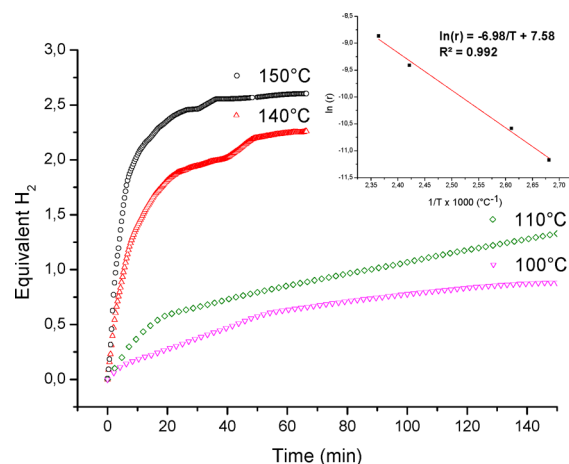


**Figure 6.** Volumetric measurements under isothermal treatment at 100, 110, 140, and 150 °C of  $\beta$ -LiHB. The inset figure is the Arrhenius plot for the determination of the apparent activation energy from the data of the volumetric measurements.

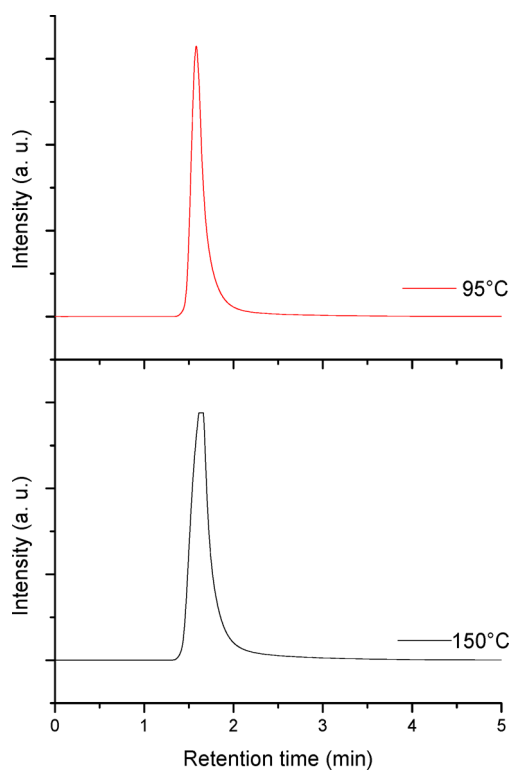


**Figure 7.** Analysis by GC of hydrogen liberated during a 2 h isothermal treatment of  $\beta$ -LiHB at 95 and 150 °C. No trace of ammonia was found in our experimental conditions, and the curves are not represented here.

by the substitution of  $\text{H}^{\delta-}$  by  $\text{Li}^+$ , with a  $\text{Li}^+\cdots\text{N}_2$  distance of 2.086(4) Å.  $\text{Li}^+$  also coordinates the terminal N atom through an interaction with the lone electron pair of N, leading to a  $\text{Li}^+\cdots\text{N}_1$  distance of 2.013(4) Å. By the same way, these two anions are connected to another  $\text{Li}^+$ , forming a cluster-like structure (Figure S1, Supporting Information). This kind of coordination is also observed in the complex  $\text{LiHB}\cdot 2\text{HB}$  (Figure S2, Supporting Information) but is not present in the  $\alpha$ -LiHB,<sup>12</sup> where the  $\text{Li}^+$  cations are bridging by two  $\text{BH}_3$  groups (Figure S3, Supporting Information). The distance between the two  $\text{Li}^+$  cations is shorter in the high-temperature

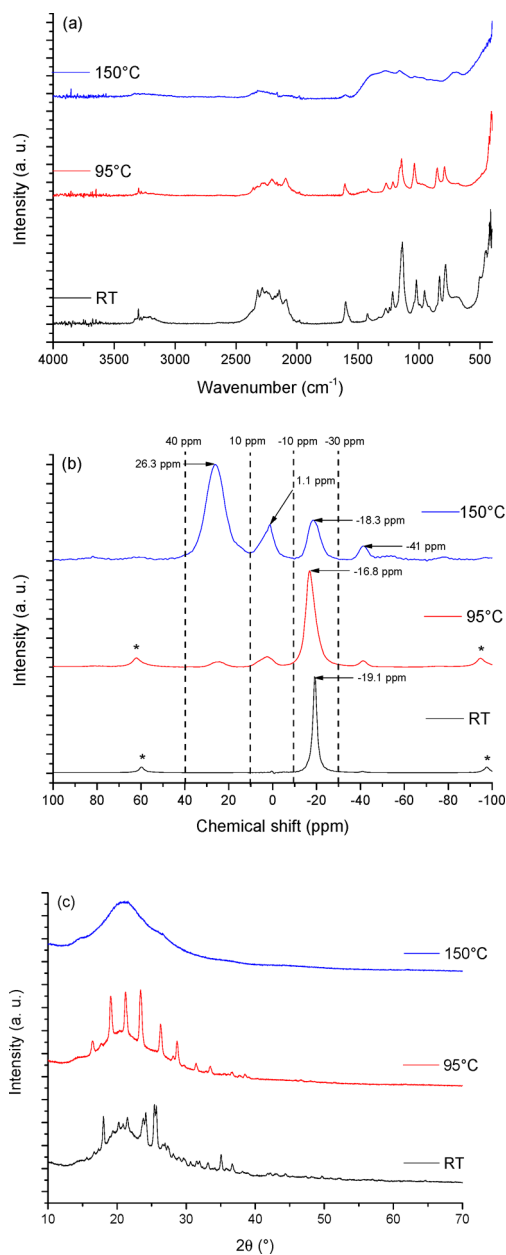


**Figure 8.** (a) FTIR and (b)  $^{11}\text{B}$  MAS NMR (spinning sidebands are indicated by \*) spectra and (c) XRD patterns of the solid residues recovered after a 2 h heat treatment of  $\beta$ -LiHB at 95 and 150 °C. For comparison, the spectrum of  $\beta$ -LiHB is also shown.

phase (3.31 Å) than in  $\beta$ -LiHB (3.49 Å), suggesting a better stability of the low-temperature phase. The  $\text{Li}^+\cdots\text{N}$  and  $\text{Li}^+\cdots\text{B}$  distances are in good agreement with previous reports on lithium amidoborane and  $\alpha$ -LiHB.<sup>12,20</sup> The tetrahedron around  $\text{Li}^+$  is slightly distorted: the angle  $\text{B}_3\cdots\text{Li}\cdots\text{B}_3$  ( $118.7(2)^\circ$ ) is more opened than the angles  $\text{N}_1\cdots\text{Li}\cdots\text{B}_3$  ( $103.8(2)^\circ$ ) and  $\text{N}_1\cdots\text{Li}\cdots\text{N}_2$  ( $109.1(2)^\circ$ ). The B–N and N–N distances are 1.549(2) and 1.495(2) Å, respectively. The former is shorter than in HB,<sup>11</sup> whereas the latter is longer, being consistent with the system of  $\text{Li}^+\cdots\text{H}^{\delta-}$  interaction inducing a reinforcement in the Lewis basicity of the  $\text{N}_2\text{H}_4$  moiety and strong electronic rearrangement due to the presence of  $\text{Li}^+$

The solid state of  $\beta$ -LiHB is stabilized by an intermolecular head-to-tail  $\text{H}^{\delta+}\cdots\text{H}^{\delta-}$  interaction (Figure 4c), with a geometry in good agreement with Klooster et al.'s definition of a

dihydrogen bond: the angle  $\text{B}_3\text{--H}_4\cdots\text{H}_7$  is bent ( $106.8^\circ$ ), whereas the  $\text{N}_1\text{--H}_7\cdots\text{H}_4$  fragment is almost linear ( $171.2^\circ$ ).<sup>21</sup> Similar contacts were also reported for HB,<sup>11</sup>  $\alpha$ -LiHB,<sup>12</sup> and NaHB.<sup>13</sup> The distance between  $\text{H}^{\delta+}$  and  $\text{H}^{\delta-}$  is 2.25 Å, longer than that for HB (2.01 Å),<sup>22</sup> but shorter than the sum of the van der Waals radii for H atoms (2.4 Å). The intermolecular head-to-tail  $\text{H}^{\delta+}\cdots\text{H}^{\delta-}$  interactions form chains (Figure 4d). For comparison, the network of dihydrogen bonds in HB extends in two dimensions and in three dimensions for AB.<sup>11,21</sup>

**Thermal Characterizations.** The TGA–MS results of  $\beta$ -LiHB are presented in Figure 5. They show that the decomposition of the borane is a five-step process. The decomposition starts at 40 °C, and over the range of 40–104 °C,  $\beta$ -LiHB liberates  $\text{H}_2$  and  $\text{N}_2$ , corresponding to a mass loss of 1.2 wt %. The second decomposition step ends at 127 °C, with 2.2 wt % of  $\text{H}_2$  being generated. The third step takes place over the range of 127–144 °C. Pure  $\text{H}_2$  (4.4 wt %) is released. For the last two steps, up to 400 °C, ca. 8.7 wt % of a mixture of  $\text{H}_2$ ,  $\text{NH}_3$ , and  $\text{N}_2$  evolves. Therefore, about 3 mol of  $\text{H}_2$  per mole of  $\beta$ -LiHB (i.e., 11.6 wt %  $\text{H}_2$ ) is generated. In our experimental conditions, no trace of  $\text{N}_2\text{H}_4$  is detected and the amount of formed  $\text{NH}_3$  is drastically decreased compared to HB. It is worth noting the absence of diborane and borazine in the gas stream (Figure S4, Supporting Information). Similar observations were reported for  $\alpha$ -LiHB and NaHB.<sup>12,13</sup> The DSC results (Figure 5) show that each of the decomposition processes is exothermic. Reversibility of H storage should then be thermodynamically difficult.<sup>8,12</sup> Another observation is that there is a slight deviation of the baseline at about 90 °C. This may be due to a phase transition.

The behavior of  $\beta$ -LiHB under prolonged isothermal heating was studied at 100, 110, 140, and 150 °C. The results of the volumetric measurements are shown in Figure 6. Three main observations stand out. First, there is no induction time: the  $\text{H}_2$  generation starts immediately. Second, the decomposition in isothermal conditions is a two-step process, with a first step that is faster than the second one. During the former step, the borane molecules are subjected to dehydrocoupling (fast intermolecular reactions) with formation of a polymeric residue and release of hydrogen. Then, the polymeric residue dehydrogenates through intramolecular reactions, with slower kinetics, since such reactions have high energy barriers and generally take place at higher temperatures under dynamic conditions.<sup>4–12</sup> Third,  $\beta$ -LiHB shows improved dehydrogenation properties in comparison to neat HB. For example, after 1 h of heating,  $\beta$ -LiHB is able to release 0.6, 0.9, 2.2, and 2.6 equiv of  $\text{H}_2$  at 100, 110, 140, and 150 °C, respectively, whereas the amount of  $\text{H}_2$  is 0.4, 1.1, and 1.4 equiv of  $\text{H}_2$  for HB at 100, 140, and 150 °C, respectively (no datum available at 110 °C for HB).<sup>11</sup> Note that the purity of  $\text{H}_2$  was determined by analyzing the gas mixture collected during the isothermal experiments at 95 and 150 °C. The results are shown in Figure 7. Unlike for HB,<sup>10,11,23</sup> no trace of ammonia was found in our conditions.

For the isothermal experiments, the rate ( $r$  in  $\text{mol H}_2 \text{ min}^{-1}$ ) of the first decomposition step was determined and then the rates were exploited to determine the apparent activation energy with the help of the Arrhenius equation. The evolution of  $\ln(r)$  as a function of  $1/T$  ( $\text{K}^{-1}$ ) is shown in Figure 6. From the slope, an apparent activation energy of  $58 \text{ kJ mol}^{-1}$  was found.

**Characterization of Solid Residues.** The solid residues forming after 2 h of isothermal treatment at 95 and 150 °C were recovered to be characterized. In Figure 8a are reported

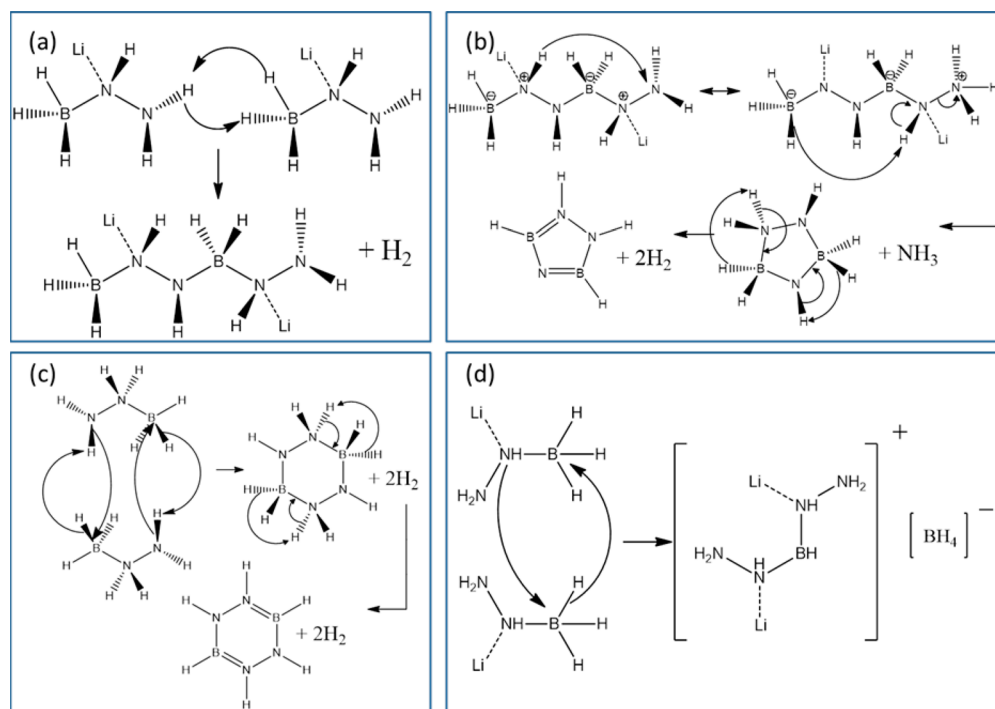


**Figure 9.** Proposition of mechanisms for the formation of monomeric units and BLHDB: (a) linear dimer with boron in  $sp^3$  hybridization; (b) 5-ring center monomer formed by proton exchange, then cyclization with  $NH_3$  release and finally dehydrocyclization, where boron is in  $sp^2$  hybridization; (c) 6-ring center monomer formed by cyclization of 2 HB monomers, followed by dehydrocyclization; (d) formation of BLHDB.

the FTIR spectra. The intensity of the N–H stretching bands ( $3390\text{--}3070\text{ cm}^{-1}$ ) has decreased for the residue formed at  $95\text{ }^\circ\text{C}$ , but these bands are no longer present for the residue formed at  $150\text{ }^\circ\text{C}$ . Similar observations can be made for the B–H stretching bands ( $2480\text{--}1900\text{ cm}^{-1}$ ), though some B–H bonds are still present for the latter residue. With respect to the bands within the range of  $1500\text{--}500\text{ cm}^{-1}$ , they have broadened. These results are explained by different dehydrogenation extents (Figure 6).

Figure 8b shows the  $^{11}\text{B}$  MAS NMR spectra of the two solid residues. For both, it seems that four species have formed as four additional signals can be distinguished. The first one peaks at  $-41\text{ ppm}$ . It is attributed to a  $BH_4^-$  environment. We assume that a compound similar to diammoniate of diborane  $[(NH_3)_2BH_2]^+[BH_4]^-$  (DADB), which is the reaction intermediate forming during the thermal decomposition of AB,<sup>24</sup> has formed. We propose the formation of bis(lithium hydrazide) of diborane  $[(LiN_2H_3)_2BH_2]^+[BH_4]^-$  (BLHDB), though further works (in progress) are required to confirm. The three other signals are visible over the ranges of  $-30$  to  $-10$ ,  $-10$  to  $10\text{ ppm}$ , and  $10\text{--}40\text{ ppm}$ . They can be ascribed to an oligo-/polymeric material with B having an  $sp^3$  hybridization (e.g.,  $NBH_2$ ), a polycyclic polymer, and a polymeric material with B showing  $sp^2$  hybridization (e.g.,  $N_2BH$  or  $N_3B$ ).<sup>24,25</sup> We, therefore, suggest that the solid residues consist of a mixture of polymers with linear and cyclic monomeric units, and species like BLHDB. For the solid residue recovered after heating  $\beta$ -LiHB at  $150\text{ }^\circ\text{C}$  for 2 h, the content of polymers with cyclic monomeric units is higher, suggesting the formation of a material with an  $N_3B$  environment.

Powder XRD was also used to analyze the solid residues (Figure 8c). After 2 h at  $95\text{ }^\circ\text{C}$ ,  $\beta$ -LiHB evolved into a material with a different crystalline structure. It transformed into  $\alpha$ -LiHB. This result is consistent with the observation made by

DSC, namely, a baseline deviation that could be due to a phase transition such as  $\beta$ -LiHB  $\rightarrow$   $\alpha$ -LiHB. The phase  $\alpha$  is thus more stable under heating. With respect to the solid residue heated at  $150\text{ }^\circ\text{C}$  for 2 h, the XRD pattern shows the formation of an amorphous material, which is the signature of a mixture of boron- and nitrogen-based polymeric species.<sup>26</sup>

**Proposition of Mechanisms.** The aforementioned results have shown that (i) the main decomposition pathway of  $\beta$ -LiHB is dehydrogenation; (ii) some ammonia is emitted under nonisothermal heating; (iii) the solid residues consist of a mixture of polymeric materials containing boron in  $sp^3$  and  $sp^2$  hybridization states; and (iv)  $BH_4^-$  is also present in the residues. We, therefore, suggest the formation of monomeric units by intermolecular reaction between  $H^{\delta-}$  and  $H^{\delta+}$ , and subsequent polycondensation of these species. Figure 9a–c shows the likely mechanisms. One path leading to the formation of  $NH_3$  is also suggested (Figure 9b). We have proposed above that the intermediate BLHDB plays a role of an activation agent in the HB decomposition; the possible mechanism of its formation is represented in Figure 9d.

## CONCLUSIONS

We have reported the synthesis and characterization results of a new crystalline phase of lithium hydrazinidoborane, called  $\beta$ -LiHB ( $\beta$ - $LiN_2H_3BH_3$ ), for chemical hydrogen storage. It was prepared from LiH and  $N_2H_4BH_3$  (HB) by mechanochemical synthesis at ambient conditions. The crystal structure of  $\beta$ -LiHB was solved in the orthorhombic space group  $Pbca$  (No. 61) with  $a = 10.25182(11)\text{ \AA}$ ,  $b = 8.47851(10)\text{ \AA}$ , and  $c = 7.46891(8)\text{ \AA}$ . Lithium hydrazinidoborane manifests two polymorphs,  $\beta$ -LiHB at low temperatures and  $\alpha$ -LiHB at high temperatures. The presence of the  $Li^+$  cation makes this material more reactive and less stable upon heating than the parent HB. Thermal and calorimetric characterizations have

shown improved dehydrogenation properties. Heated at 5 °C min<sup>-1</sup>,  $\beta$ -LiHB is able to release about 11.6 wt % H<sub>2</sub> up to 400 °C, with drastically reduced amounts of unwanted byproducts, such as N<sub>2</sub>H<sub>4</sub> and NH<sub>3</sub>. In isothermal conditions, at 150 °C, about 10 wt % of pure H<sub>2</sub> is generated in less than 1 h, with a real improvement in terms of dehydrogenation kinetics. From analyses of the released gases and solid residues, the dehydrogenation paths are discussed. The appearance of bis(lithium hydrazide) of diborane [(LiN<sub>2</sub>H<sub>3</sub>)<sub>2</sub>BH<sub>2</sub>]<sup>+</sup>[BH<sub>4</sub>]<sup>-</sup>, acting as an activation intermediate, and formation of polymeric residues constituted of linear and cyclic monomeric units are suggested. Works are in progress to better identify the different species. To conclude, we show that  $\beta$ -LiHB has a potential for chemical hydrogen storage if combined with an adapted effective recycling process of the solid residues.

## ■ ASSOCIATED CONTENT

### Supporting Information

The atomic positions for  $\beta$ -LiHB (Table S1), the representations of the various cluster-like structures of LiHB-based materials (Figures S1–S3), and MS results of the thermal decomposition of  $\beta$ -LiHB (Figure S4). This material is available free of charge via the Internet at <http://pubs.acs.org>.

## ■ AUTHOR INFORMATION

### Corresponding Author

\*E-mail: [umit.demirci@um2.fr](mailto:umit.demirci@um2.fr).

### Author Contributions

All authors have given approval to the final version of the manuscript.

### Notes

The authors declare no competing financial interest.

## ■ ACKNOWLEDGMENTS

The authors would like to acknowledge the support of the Direction Générale des Armées (DGA, France), the Centre National de la Recherche Scientifique (CNRS, France), and Fonds de la Recherche Scientifique (FNRS, Belgium). U.B.D. and T.I. would like to thank the JSPS (Japan) for partially supporting the present work through the JSPS Summer Program given to R.M. Also, U.B.D. and Y.F. would like to thank the COST program MP1103 called “Nanostructured Materials for Solid-State Hydrogen Storage” for partially supporting the present work through the short-term scientific mission given to R.M. Finally, Y.F. and R.M. acknowledge the SNBL (ESRF, France) for the beam-time.

## ■ REFERENCES

- (1) Armaroli, N.; Balzani, V. *ChemSusChem* **2011**, *4*, 21–36.
- (2) *Targets for Onboard Hydrogen Storage Systems for Light-Duty Vehicles*; U.S. Department of Energy: Washington, DC, 2009; <http://www1.eere.energy.gov>.
- (3) Demirci, U. B.; Miele, P. *Energy Environ. Sci.* **2009**, *2*, 627–637.
- (4) Staubitz, A.; Robertson, A. P. M.; Manners, I. *Chem. Rev.* **2010**, *110*, 4079–4124.
- (5) Baitalov, F.; Baumann, J.; Wolf, G.; Jaenicke-Rossler, K.; Leitner, G. *Thermochim. Acta* **2002**, *391*, 159–168.
- (6) Carpenter, J. D.; Ault, B. S. *Chem. Phys. Lett.* **1992**, *197*, 171–174.
- (7) (a) Gutowska, A.; Li, L.; Shin, Y.; Wang, C. M.; Li, X. S.; Linehan, J. C.; Smith, R. S.; Kay, B. D.; Schmid, B.; Shaw, W.; Gutowski, M.; Autrey, T. *Angew. Chem., Int. Ed.* **2005**, *44*, 3578–3582. (b) Goettker-Schnetmann, L.; White, P.; Brookhart, M. *J. Am. Chem. Soc.* **2004**, *126*, 1804–1811. (c) Bluhm, M. E.; Bradley, M. G.; Butterick, R., III;

Kusari, U.; Sneddon, L. G. *J. Am. Chem. Soc.* **2006**, *128*, 7748–7749. (d) Benzouaa, R.; Demirci, U. B.; Chiriac, R.; Toche, F.; Miele, P. *Thermochim. Acta* **2010**, *509*, 81–86.

(8) Xiong, Z.; Yong, C. K.; Wu, G.; Chen, P.; Shaw, W.; Karkamkar, A.; Autrey, T.; Jones, M. O.; Johnson, S. R.; Edwards, P. P.; David, W. I. F. *Nat. Mater.* **2008**, *7*, 138–141.

(9) Fijalkowski, K. J.; Grochala, W. *J. Mater. Chem.* **2009**, *19*, 2043–2050.

(10) Hügle, T.; Kühnel, M. F.; Lentz, D. *J. Am. Chem. Soc.* **2009**, *131*, 7444–7446.

(11) Moury, R.; Moussa, G.; Demirci, U. B.; Hannauer, J.; Bernard, S.; Petit, E.; van der Lee, A.; Miele, P. *Phys. Chem. Chem. Phys.* **2012**, *14*, 1768–1777.

(12) Wu, H.; Zhou, W.; Pinkerton, F. E.; Udovic, T. J.; Yildirim, T.; Rush, J. *J. Energy Environ. Sci.* **2012**, *5*, 7531–7535.

(13) Moury, R.; Demirci, U. B.; Ichikawa, T.; Filinchuk, Y.; Chiriac, R.; van der Lee, A.; Miele, P. *ChemSusChem* **2013**, *6*, 667–673.

(14) Armstrong, D. R.; Perkins, P. G.; Walker, G. T. *J. Mol. Struct.: THEOCHEM* **1985**, *122*, 189–204.

(15) Favre-Nicolin, V.; Cerny, R. *J. Appl. Crystallogr.* **2002**, *35*, 734–743.

(16) Petricek, V.; Dusek, M.; Palatinus, L. *Jana2006: The Crystallographic Computing System*; Institute of Physics, Academy of Sciences: Praha, Czech Republic, 2006.

(17) Filinchuk, Y.; Chernyshov, D.; Černý, R. *J. Phys. Chem. C* **2008**, *112*, 10579–10584.

(18) Filinchuk, Y.; Hagemann, H. *Eur. J. Inorg. Chem.* **2008**, 3127–3133.

(19) (a) Hartman, M. R.; Rush, J. J.; Udovic, T. J.; Bowman, R. C., Jr.; Hwang, S.-J. *J. Solid State Chem.* **2007**, *180*, 1298–1305. (b) Filinchuk, Y.; Chernyshov, D.; Nevidomskyy, A.; Dmitriev, V. *Angew. Chem., Int. Ed.* **2008**, *47*, 529–532.

(20) Wu, H.; Zhou, W.; Yildirim, T. *J. Am. Chem. Soc.* **2008**, *130*, 14834–14839.

(21) Klooster, W. T.; Koetzle, T. F.; Siegbahn, P. E. M.; Richardson, T. B.; Crabtree, R. H. *J. Am. Chem. Soc.* **1999**, *121*, 6337–6343.

(22) Mebs, S.; Grabowsky, S.; Förster, D.; Kickbusch, R.; Hartl, M.; Daemen, L. L.; Morgenroth, W.; Luger, P.; Paulus, B.; Lentz, D. *J. Phys. Chem. A* **2010**, *114*, 10185–10196.

(23) Goubeau, J.; Ricker, E. Z. *Anorg. Allg. Chem.* **1961**, *310*, 123–142.

(24) Stowe, A. C.; Shaw, W. J.; Linehan, J. C.; Schmid, B.; Autrey, T. *Phys. Chem. Chem. Phys.* **2007**, *9*, 1831–1836.

(25) (a) Gervais, C.; Framery, E.; Duriez, C.; Maquet, J.; Vaultier, M.; Babonneau, F. *J. Eur. Ceram. Soc.* **2004**, *25*, 129–135. (b) Shimoda, K.; Zhang, Y.; Ichikawa, T.; Miyaoka, H.; Kojima, Y. *J. Mater. Chem.* **2011**, *21*, 2609–2615. (c) Kim, D.-P.; Moon, K.-T.; Kho, J.-G.; Economy, J.; Gervais, C.; Babonneau, F. *Polym. Adv. Technol.* **1999**, *10*, 702–712.

(26) Hu, M. G.; Geanangel, R. A.; Wendlandt, W. W. *Thermochim. Acta* **1978**, *23*, 249–255.